Kontagora Journal of Mathematics(KJM)
Volume 1, Issue 1, September 2025
https://fuekjournals.org/index.php/KJM

Unsteady Couette Flow in a Composite Channel with Porous and Clear Regions Using Caputo–Fabrizio Fractional Derivative Approach

Shehu A. Muhammad[1*]; Muhammad L. Kaurangini[2] ; Kabir L. Yusuf[3]; Muhammad K. Musa[3]

Corresponding Author: shehukurami65@gmail.com

[1*] *Mathematics Department, School of Basic and Remedial, Ahmadu Bello University, Zaria.*

[2] *Mathematics Department, Aliko Dangote University of Science and Technology, wudil*

[3] *Mathematics Department, Ahmadu Bello University, Zaria.*

DOI: https://doi.org/**10.5281/zenodo.17364996**

Abstract

This study examines fully developed unsteady Couette flow in a composite channel partially filled with a porous medium and partially with a clear fluid, within a fractional derivative framework. The Brinkman-extended Darcy model governs the porous region, while the Stokes equation describes the clear region, both formulated using Caputo–Fabrizio fractional derivatives to account for memory effects. The governing equations are transformed via Laplace techniques, solved analytically in the Laplace domain, and inverted to the time domain using the Riemann-sum approximation. Compared with classical integer-order models, the fractional-order formulation provides a more comprehensive and physically realistic description of the flow. Parametric analysis explores the effects of fractional order, time, and other physical parameters on velocity, interfacial velocity, skin friction, and volumetric flow rate. Results, presented as MATLAB-generated contour plots, reveal that transient and interfacial velocities and flow rate increase with time, whereas skin friction decreases. These findings demonstrate the effectiveness of fractional calculus in capturing the complex dynamics of fluid flow in composite domains.

Keywords: Unsteady Couette-Flow, Composite channel, Fractional Derivative, Caputo-Fabrizio

Nomenclature

u_f' Dimensional velocity in the clear fluid region.

u_p' Dimensional velocity in the porous medium region.

u_f Dimensionless velocity in the clear fluid region.

u_p Dimensionless velocity in the porous medium region.

U_i Interfacial velocity in dimensionless form.

y' Dimensional y coordinate.

y Dimensionless y coordinate.

ρ Density of the fluid.

β Stress jump coefficient.

Da Darcy number.

υ_f Kinematics viscosity of the fluid.

υ_e Effective kinematics viscosity of the fluid saturated porous material.

F Tangential momentum accommodation coefficient.

β_v Dimensionless variable.

Kn Kundsen number.

λ Molecular mean free path.

k Permeability of the porous material.

d Interfacial position.

u_{ti} Transient interfacial velocity.

u_t Transient velocity.

$\tau_{0,1,d}$ Skin friction at the wall of the porous medium.

$\tau_{11,d1}$ Skin friction at the wall of the clear fluid region.

α Fractional parameter.

Q_f Mass flux of the clear fluid.

Q_p Mass flux of the porous fluid.

Introduction

Fractional calculus has emerged as a powerful mathematical tool for modelling complex physical phenomena, particularly in engineering and applied mathematics. Unlike classical integer-order models, fractional derivatives inherently incorporate memory and hereditary properties of materials and processes, enabling a more accurate description of real-world systems. In fluid dynamics, fractional-order formulations often demonstrate closer agreement with experimental data than their integer-order counterparts, especially in porous media applications. This improvement stems from the fact that conventional differential equations are often unable to capture the intricate behaviour and long-term memory effects present in such systems. By generalizing differentiation and integration to non-integer (real or complex) orders, fractional calculus bridges the conceptual gap between these operations, offering greater flexibility and realism in modeling. Fluid flow through composite channels is of particular interest due to its broad engineering applications, including geothermal energy extraction, crude oil recovery, metal casting, and industrial separation processes. The complex nature of such flows has inspired extensive research efforts. Investigating fluid flow through porous passages with different permeabilities, Yadav et al (2023) analysed the flow model which often occurs in crude oil extraction, blood flow in the arteries, filtration of underground different fluids flowing together. Shaheen et al (2024) observed that in an unsteady mathematical model Couette flow of Jeffrey fluid through parallel plates where the upper plate moves with uniform velocity while lower plate kept constant, the velocity profile enhances with Darcy number for both simple and generalized Couette flows.

The influence of transient changes in porous structure was highlighted by Oni et al. (2022), who showed that sudden insertion or removal of the porous medium significantly affects the time to reach steady state, skin friction, and volumetric flow rate. Unsteady behaviour in composite channels has also been examined by Jha and Odengle (2015), who analysed unsteady Couette flow in a partially porous channel using a semi-analytical approach. Their study revealed strong agreement between steady-state analytical results and numerical solutions of the unsteady problem, obtained via implicit finite-difference and Riemann-sum approximation at large times. Comparable consistency between steady and unsteady results was also reported by Kaurangini and Jha (2011) in their work on unsteady generalized Couette flow in composite microchannels. Ranjbarzadeh and Sappa, (2025) reviewed fluid flow and heat transfer in porous media, combining theoretical, numerical, and experimental approaches. The study highlights key models—Darcy's law, the Brinkman equation, and volume-

averaging methods—while addressing challenges like heterogeneity, anisotropy, and scale effects. By integrating experiments with simulations, the work underscores their complementary value in advancing porous media research. Verma and Datta (2012) studied viscous incompressible fluid flow through a heterogeneous porous medium with linearly varying permeability, identifying the significant influence of transverse permeability variation. In another studies, Singh and Verma (2020) provided exact expressions for velocity, volumetric flow rate, and shear stress in cylindrical geometries, underscoring the importance of permeability and channel gap.

The versatility of fractional derivatives in modelling such systems has been well documented. Hussain et al (2023) presented a computational analysis taken into account the effects of porous layer on the flow dynamics, heat transfer and hydrodynamic forces of hybrid Nano fluid in a channel having an open cavity fixed with bottom wall in the presence of partial magnetic field. More recently, Daud et al. (2022) applied Caputo fractional derivatives to model convective Casson fluid flow in a microchannel with thermal radiation, showing that velocity and temperature profiles increase with fractional order (α) and radiation parameter (R), but decrease with higher viscosity ratio (β_v).

Building on this body of work, the present study investigates unsteady Couette flow in a composite channel comprising both porous and clear regions, with one plate in motion and the other fixed. Employing the Caputo–Fabrizio fractional derivative formulation, we analyse the effects of key physical parameters on velocity profiles, interfacial velocity, mass flux, and skin friction. The resulting trends are presented and interpreted through detailed graphical analysis. Despite extensive studies on unsteady Couette flow in porous channels, most existing models rely on classical integer-order formulations that cannot capture memory and hereditary effects inherent in real systems. Fractional-order approaches have been applied to single-region channels and specialized fluids, but the case of composite channels containing both porous and clear regions remains largely unexplored. To address this gap, the present study applies the Caputo–Fabrizio fractional derivative to investigate unsteady Couette flow in a composite channel with one plate in motion and the other fixed. By incorporating fractional-order memory effects, porous resistance, and moving boundary conditions, the work provides semi-analytical solutions and detailed graphical analyses of velocity, interfacial velocity, skin friction, and mass flux. This contribution extends fractional calculus applications to composite channel flows thereby offering deeper insights into their transient dynamics.

Mathematical Modeling

A fully developed study fractional derivative of unsteady fluid flow in a horizontal parallel-plate channel partially filled with porous material and partially filled with a clear fluid is considered. The schematic diagram of the channel in consideration is shown in the figure below.

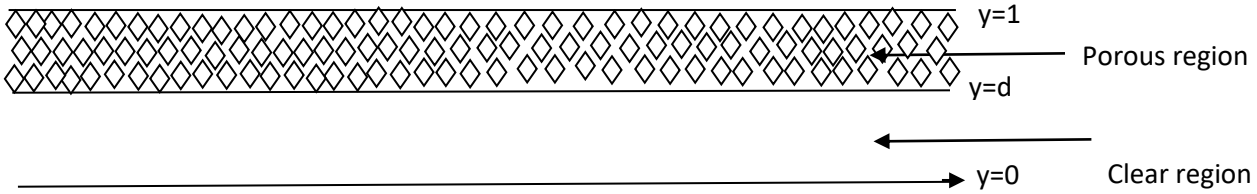

Figure 1: Show the schematic diagram of the fluid flow in the microchannel.

The equation of the fluid flow in the porous layer is obtained using the Brinkman extended Darcy equation and the equation of the fluid flow for the clear fluid region is obtained by the Stokes equation. The lower plate is considered to be moving at time $t > 0$ and the other one is at rest at time $t \leq 0$. The governing equations in dimensionless form are as follows:

$$\frac{\partial^{\alpha} u_f}{\partial t^{\alpha}} = \frac{\partial^2 u_f}{\partial y^2} \tag{1}$$

$$\frac{\partial^{\alpha} u_p}{\partial t^{\alpha}} = \gamma \frac{\partial^2 u_p}{\partial y^2} - \frac{u_p}{Da} \tag{2}$$

The non-dimensional parameters are as follows:

$$\left.\begin{aligned} & u_f = \frac{u_f'}{u}, \quad u_p = \frac{u_p'}{u}, \quad y = \frac{y'}{h'} \quad d = \frac{d'}{h'} \quad y = \frac{t'\nu}{h^2} \\ & \gamma = \frac{\nu_e}{\nu_p} \quad Da = \frac{k'}{h^2}\beta_v = \frac{2-F}{F} \end{aligned}\right\} \tag{3}$$

The Initial and boundary condition are:

$$\left.\begin{aligned} & t \leq 0: \quad u_f = 0, \quad u_p = 0, \quad for\ 0 \leq y \leq 1 \\ & t > 0: \quad u_f = 1, \quad at \quad y = 0 \\ & u_p = 0, \quad at \quad y = 1 \\ & u_f = u_p = u_i \\ & \gamma \frac{\partial u_p}{\partial y} - \frac{\partial u_f}{\partial y} = \frac{\beta}{\sqrt{Da}} u_p \qquad at \quad y = d \end{aligned}\right\} \tag{4}$$

Applying Laplace transformation techniques and using Caputo-Fabrizio method of solving fractional-order derivatives to equations (1) and (2) above

We have,

$$\frac{d^2u_f}{dy^2} - \frac{asu_f}{s+b} = 0 \tag{5}$$

$$\frac{d^2u_p}{dy^2} - \left(\frac{as}{s+b}\right)u_p = 0 \tag{6}$$

Applying the initial and boundary condition in equation (4) above.

Then, equations (5) and (6) are solved as follows:

$$\bar{u}_f(y,s) = \frac{\frac{1}{s}\sinh(A(d=1))}{\sinh(Ad)} + \frac{U_i\sinh(Ay)}{\sinh(Ad)} \tag{7}$$

$$\bar{u}_p(y,s) = \frac{U_i\sinh(A(1-y))}{\sinh(B(1-d))} \tag{8}$$

At the interface,

$$\gamma\frac{du_p}{dy} - \frac{du_f}{dy} = \frac{\beta}{\sqrt{Da}}U_i \qquad At\ y = d \tag{9}$$

$$\frac{du_f}{dy} = \frac{1}{\sinh(Ad)}\left(U_i\cosh(Ay) - \frac{1}{s}\cosh\big(A(d-y)\big)\right) \tag{10}$$

$$\frac{du_p}{dy} = \frac{BU_i}{\sinh(A(d-1))}\cosh(B(y-1)) \tag{11}$$

By substituting equations (10) and (11) into equation (9) this is solved to give:

$$U_i = \frac{\frac{-A}{s\sinh(Ad)}}{\gamma B\left(\frac{\cosh(B(d-1))}{\sinh(B(1-d))}\right) - \frac{Acosh(Ad)}{\sinh(Ad)} - \frac{\beta}{\sqrt{Da}}} \tag{12}$$

Where: A $= \sqrt{\frac{as}{s+b}}$; B $= \sqrt{\frac{1}{\gamma}}(\frac{1}{Da} - \frac{as}{s+b})$;$c_1 = \frac{1}{s}$; $c_2 = \frac{Ui - \frac{1}{s}\cosh(Ad)}{\sinh(Ad)}$

$$c_3 = \frac{Ui\sinh(B)}{\sinh(B(1-d))} \ ;\ c_4 = \frac{Uicosh(B)}{\sinh(B(1-d))}$$

Steady State

$$\frac{d^2u_f}{dy^2} = 0 \tag{13}$$

$$\frac{d^2u_p}{dy^2} - \frac{u_p}{Da} = 0 \tag{14}$$

Equation (13) is integrated twice to give:

$$u_f(y) = k_1 y + k_2 \tag{15}$$

Similarly, equation (14) is solved as:

$$u_p(y) = k_3 \cosh(Fy) + k_4 \sinh(Fy) \tag{16}$$

Where: $F = \frac{1}{\sqrt{\gamma Da}}$, $k_1 = \frac{U_i - 1}{d}$, $k_2 = 1, k_3 = \frac{U_i \sinh(F)}{\sinh(F(1-d))}$,

$k_4 = \frac{-U_i \cosh(F)}{\sinh(F(1-d))}$

At the interface,

$$\gamma \frac{du_p}{dy} - \frac{du_f}{dy} = \frac{\beta}{\sqrt{Da}} U_i \qquad At\ y = d \tag{17}$$

$$\frac{du_f}{dy} = k_1 \tag{18}$$

$$\frac{du_p}{dy} = F(k_3 \cosh(Fd) + k_4 \sinh(Fd)) \tag{19}$$

Now, substituting equations (18) and (19) into equation (17) which is solved to give:

$$U_i = \frac{1}{d\left(\gamma F coth\left(F(1-d)\right)\right) + \frac{1}{d} + \frac{\beta}{\sqrt{Da}}} \tag{20}$$

Skin Friction (Transient State)

Skin friction refers to the tangential (shear) force per unit area exerted by a fluid on a solid boundary due to viscosity. It arises from the velocity gradient at the wall and is directly related to the rate of momentum transfer between fluid layers and the boundary surface. The skin friction is the derivative of the solution of the velocity. The calculated skin friction is given by:

$$\overline{u}_f(y, s) = \frac{\frac{1}{s}\sinh(A(d=1))}{\sinh(Ad)} + \frac{U_i \sinh(Ay)}{\sinh(Ad)} \tag{21}$$

$$\overline{u}_p(y, s) = \frac{U_i \sinh(A(1-y))}{\sinh(B(1-d))} \tag{22}$$

By differentiating equations (21) and (22) respectivelythe results obtained are:

$$\overline{\tau}_f = \frac{1}{\sinh(Ad)}\left(U_i \cosh(Ay) - \frac{1}{s}\cosh\left(A(d-y)\right)\right) \tag{23}$$

And

$$\overline{\tau}_p = \frac{BU_i}{\sinh(A(d-1))}\cosh(B(y-1)) \quad (24)$$

Now,

$$\overline{\tau}_{f\ y=0} = \frac{1}{\sinh(Ad)}\left(U_i - \frac{1}{s}\cosh\left(A(d)\right)\right) \quad (25)$$

$$\overline{\tau}_{f\ y=d} = \frac{1}{\sinh(Ad)}\left(U_i\cosh(Ad) - \frac{1}{s}\right) \quad (26)$$

And

$$\overline{\tau}_{p\ y=d} = \frac{BU_i}{\sinh(A(d-1))}\cosh(B(d-1)) \quad (27)$$

$$\overline{\tau}_{p\ y=1} = \frac{BU_i}{\sinh(A(d-1))} \quad (28)$$

Mass Flux (Transient State)

The mass flux is the integral of the solution of the velocity, that is:

$$Q_f = \int_0^d \left(\frac{\frac{1}{s}\sinh\left(A(d=1)\right)}{\sinh(Ad)} + \frac{U_i\sinh(Ay)}{\sinh(Ad)}\right)dy \quad (29)$$

$$Q_p = \int_d^1 \left(\frac{U_i\sinh\left(A(1-y)\right)}{\sinh\left(B(1-d)\right)}\right)dy \quad (30)$$

Equations (29) and (39) are solved to give:

$$Q_f = \frac{1}{Asinh(Ad)}\left(\frac{1}{s}(\cosh(Ad)-1) + U_i(\cosh(Ad)-1)\right) \quad (31)$$

$$Q_p = \frac{U_i}{Bsinh\left(B(d-1)\right)}(1-\cosh(B(d-1))) \quad (32)$$

$$Q = Q_f + Q_p$$

$$Q = \frac{1}{Asinh(Ad)}\left(\frac{1}{s}(\cosh(Ad)-1) + U_i(\cosh(Ad)-1)\right) + \frac{U_i}{Bsinh\left(B(d-1)\right)}(1-\cosh(B(d-1))) \quad (33)$$

Skin Friction (Steady State)

$$\overline{u}_f(y) = \left(\frac{U_i-1}{d}\right)y + 1 \quad (34)$$

$$\overline{u}_p(y) = \frac{U_i\sinh(F(y-1))}{\sinh(F(d-1))} \quad (35)$$

Differentiating equations (34) and (35) gives:

$$\frac{d\bar{u}_f}{dy} = \frac{U_i - 1}{d} \quad (36)$$

$$\frac{d\bar{u}_p}{dy} = \frac{U_i F \cosh(F(y-1))}{\sinh(F(d-1))} \quad (37)$$

Now,

$$\tau_{sf} \quad _{y=0} = \frac{U_i - 1}{d} (38)$$

$$\tau_{sf} \quad _{y=d} = \frac{U_i - 1}{d} \quad (39)$$

And

$$\tau_{sp} \quad _{y=d} = \frac{U_i F \cosh(F(d-1))}{\sinh(F(d-1))} \quad (40)$$

$$\tau_{sp} \quad _{y=1} = \frac{U_i F}{\sinh(F(d-1))} \quad (41)$$

Mass Flux (Steady State)

$$Q_{sf} = k_1 \int_0^d y \, dy + k_2 \int_0^d dy \quad (42)$$

$$Q_{sp} = \int_d^1 \frac{U_i \sinh(F(d-1))}{\sinh(F(d-1))} dy \quad (43)$$

Equations (42) and (43) are solved as:

$$Q_{sf} = d\left(\frac{k_1 d}{2} + k_2\right) \quad (44)$$

$$Q_{sp} = \frac{U_i}{F\sinh(F(d-1))}(1 - \cosh(F(d-1))) \quad (45)$$

$$Q = Q_{sf} + Q_{sp}$$

$$Q = d\left(\frac{k_1 d}{2} + k_2\right) + \frac{U_i}{F\sinh(F(d-1))}(1 - \cosh(F(d-1))) \quad (46)$$

Results and Discussion

The results obtained from the analytical solution of the governing equations of the unsteady Couette-flow in a composite channel partially filled with porous material and partially with a clear fluid are inverted into time domain by Riemann-sum approximation and are represented in line graphs which are obtain from MatLab (2016) software programme. The effects of the parameters involve in this work with different values are extensively discussed. The line graphs obtained are for the transient

velocity, interfacial velocity, skin friction and volume flow rate of the fluid flow, these are obtained using MatLab (2016) software program as shown below.

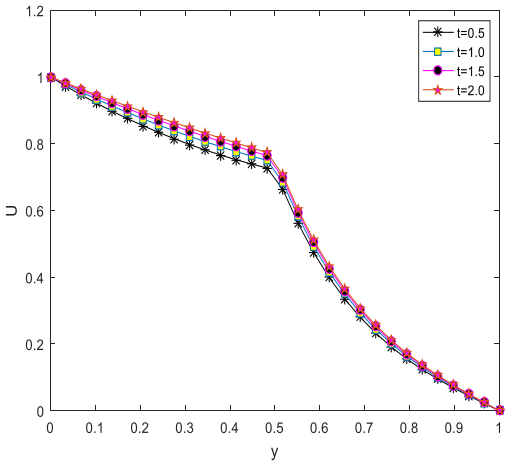

Fig1:Transient velocity profiles for different values of t and y with ($Da = 0.1\ \gamma = 0.5; d = 0.5; \beta = -0.9$)

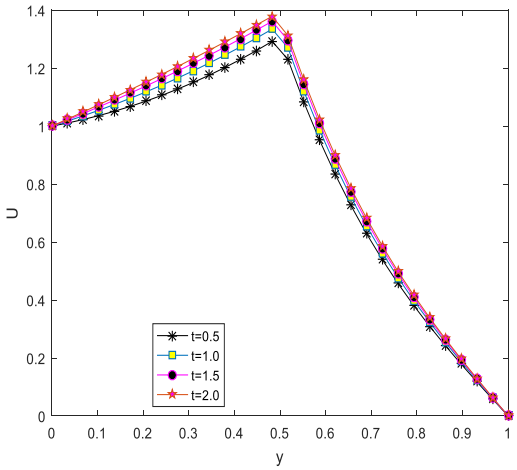

Fig2:Transient velocity profiles for different values of t and y with ($Da = 0.01;\ \gamma = 1.0; d = 0.5;\ \beta = -0.9$)

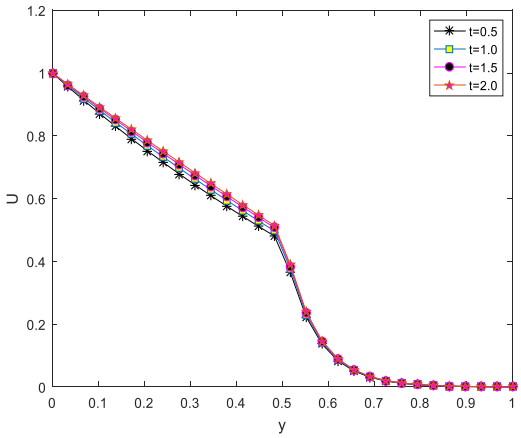

Fig3: Transient velocity profiles for different values of t with y with($Da = 0.001;\ \gamma = 0.5; d = 0.5;\ \beta = -0.9$)

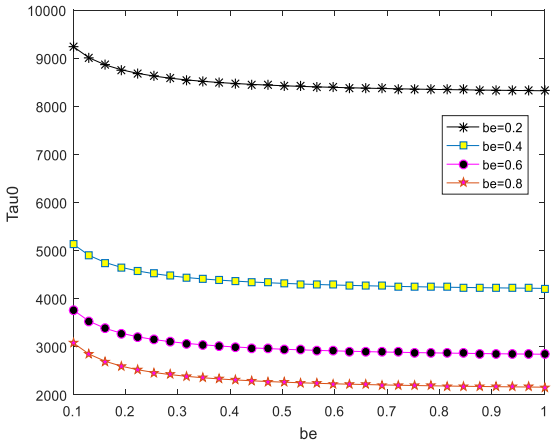

Fig4: Skin friction of the velocity with different values of t and $\beta$with ($Da = 0.01;\ \gamma = 1.0; d = 0.1;\ y = 1.0$)

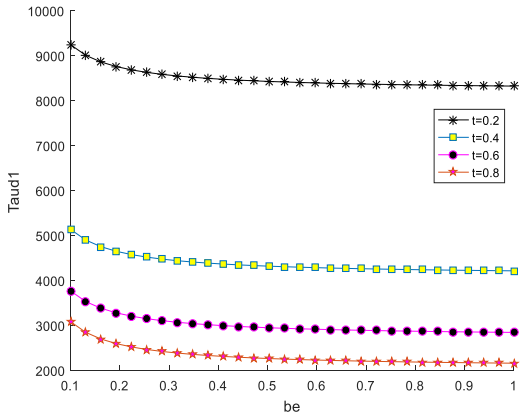

Fig5:Skin friction of the velocity with different values of t ($Da = 0.01;\ \gamma = 1.0; d = 0.1;\ y = 1.0$)

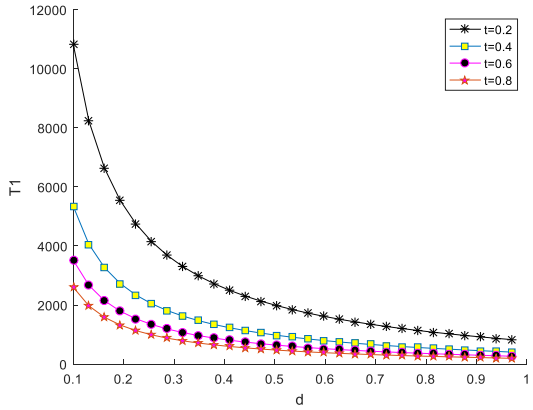

Fig6: Skin friction of the velocity with different values of t and β with and d with ($Da = 0.001;\ \gamma = 1.0; \beta = -0.4;\ y = 0.5$)

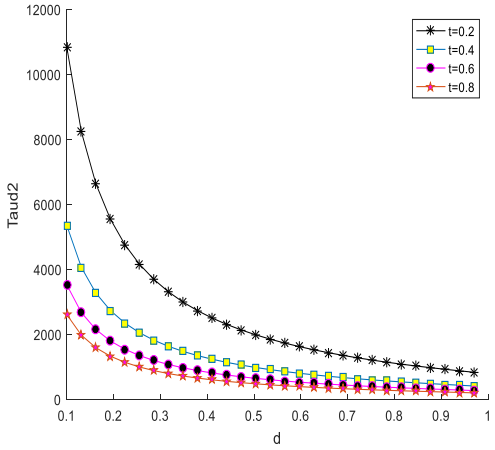

Fig7: Skin friction of the velocity with different values of t and d with ($Da = 0.001;\ \gamma = 1.0; \beta = -0.4;\ y = 0.5$)

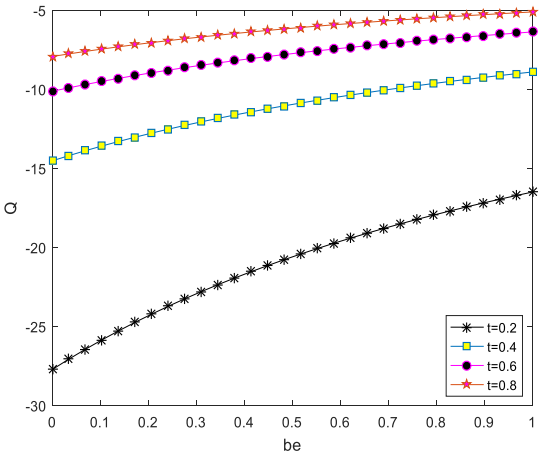

Fig8: Mass flux profiles for velocity with different values of t and β with($Da = 0.1;\ \gamma = 1.0; d = 0.5;\ y = 0.5$)

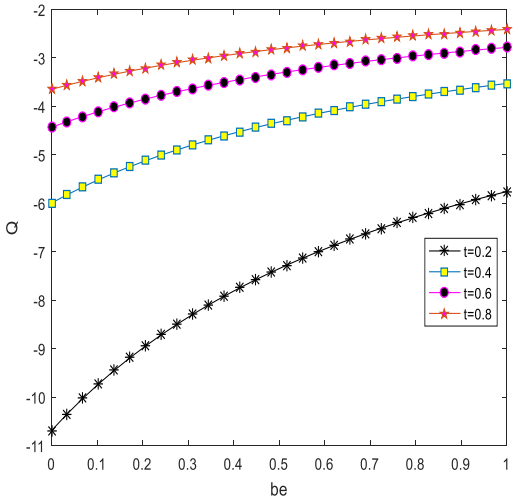

Fig8(b): Mass flux profiles for velocity with different values of ($Da = 0.1;\ \gamma = 1.0; d = 0.5;\ y = 0.5$)

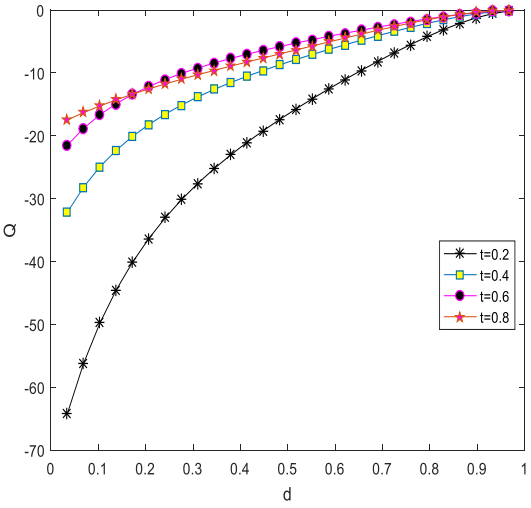

Fig9(a): Mass flux profiles for velocity with different values of t and d with ($Da = 0.1;\ \gamma = 0.5; \beta = 0.1;\ y = 0.5$)

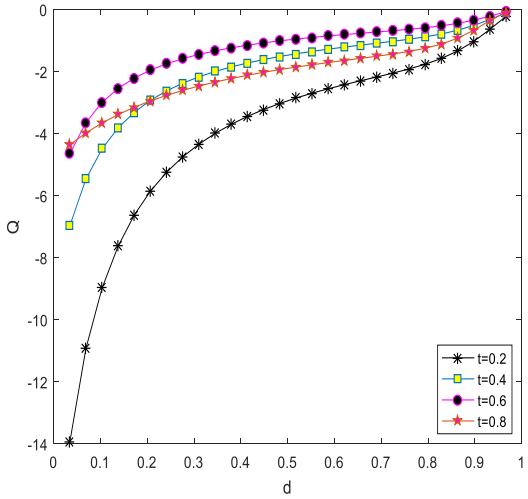

Fig9(b): Mass flux profiles for velocity with different values of t and β with ($Da = 0.1;\ \gamma = 0.5; d = 0.5;\ y = 0.5$)

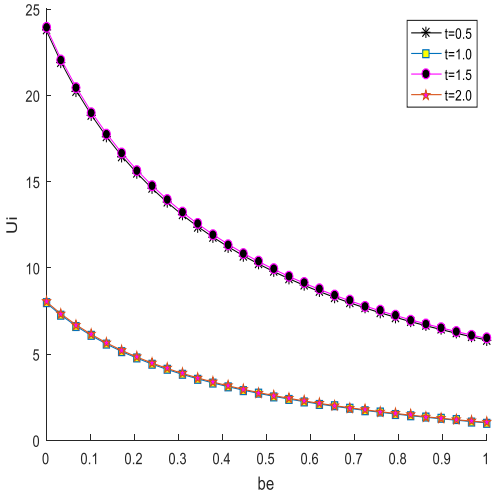

Fig10(a): Interfacial velocity profiles for different values of t and d with ($Da = 0.1;\ \gamma = 0.5; \beta = 0.1;\ y = 0.5$)

t and d with $(Da = 0.01;\ \gamma = 1.0; \beta = 0.1;\ y = 0.5)$of t and β with $(Da = 0.1;\ \gamma = 1.0; d = 0.5;\ y = 0.4)$

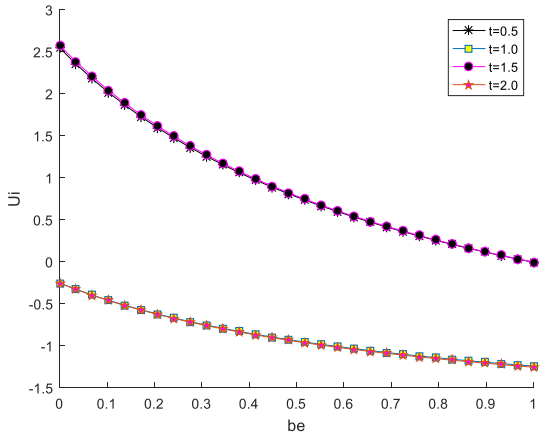

Fig10(b):Interfacial velocity profiles for different values of t and β with $(Da = 0.01;\ \gamma = 1.0; d = 0.5;\ y = 0.4)$

Figures1–3 present the transient velocity profiles $u(y,t)$ for various times t and taking into account the following representative parameter values for figures 1, 2 and 3 respectively: $(Da = 0.1\ \gamma = 0.5; d = 0.5; \beta = -0.9), (Da = 0.01;\ \gamma = 1.0; d = 0.5;\ \beta = -0.9)$ and$(Da = 0.001;\ \gamma = 0.5; d = 0.5;\ \beta = -0.9)$. It is interesting to note that in all cases, the velocity profiles increase monotonically with time, indicating that momentum from the moving plate diffuses progressively through the fluid–porous system until a steady distribution is approached.

For larger Darcy number ($Da = 0.1$, Figure 1), the porous medium offers less resistance to flow, enabling faster penetration of motion into the porous region. Consequently, at any given$t$, the velocity throughout the channel is higher compared to the lower-Da cases. The velocity gradient at the interface is relatively small, reflecting more effective momentum coupling between the clear and porous layers. For the intermediate Darcy number ($Da = 0.01$, Figure 2), the reduced permeability slows the transmission of motion into the porous medium. This manifests as noticeably lower velocities in the porous region at early and intermediate times, with a sharper velocity drop at the interface. The slightly larger $\gamma = 1.0$ in this case (compared to $\gamma = 0.5$ in Figures. 1 and 3) influences the viscous coupling and interfacial shear, producing steeper near-wall gradients in the clear region. At the lowest Darcy number ($Da = 0.001$, Figure 3), the porous layer behaves almost like a solid barrier. The velocity in the porous region remains very small even at later times, and the profile in the clear region resemble that of a single-phase Couette flow over a nearly impermeable

surface. The large interfacial shear indicates strong resistance at the boundary between the two regions. Across all three figures, the increase of velocity with time is a direct result of the start-up nature of the problem: the impulsively started plate gradually transfers momentum to the fluid, with the rate of penetration governed primarily by the permeability Da, the viscous coupling parameter γ and the fractional time derivative kernel (here embedded in the transient response). Lower Da values delay the equilibration process, keeping velocities suppressed in the porous region for longer durations. These trends are consistent with earlier composite-channel studies (e.g., Jha and Odengle 2014; Singh and Verma 2020), where reduced permeability and higher viscous resistance were shown to slow transient development and steepen interfacial velocity gradients.

Figures 4 and 5 depict the skin friction τ_0 and τ_d at the porous-fluid interface for different values of t and slip parameter β using $Da = 0.01, \gamma = 1.0, d = 0.1, y = 1.0$. In both cases, skin friction decreases as t increases. This decay reflects the reduction in shear stresses over time as the transient flow approaches a steady state. The influence of β is linked to wall slip: higher slip (β large) weakens the no-slip constraint, reducing shear at the interface and thus lowering τ. Figures 6 and 7 show the skin friction τ_1 and τ_d for the clear-fluid region for varying t and d, with $Da = 0.001, \gamma = 1.0, \beta = -0.4, y = 0.5$. Here again, skin friction decreases with time, consistent with the dissipation of initial velocity gradients. The parameter d, representing geometric or scale effects between the porous and clear regions, influences the interfacial coupling: larger d values typically alter the effective shear layer thickness, impacting the decay rate of skin friction.

Figures 8(a) and (b) illustrate the volume flow rate profiles for varying t andβ, with$Da = 0.1, \gamma = 1.0, d = 0.5, y = 0.5$. The flow rate increases with time, as expected from the corresponding velocity trends in Figs 1–3. The slip parameter β modulates this increase: higher slip enhances flow rate by reducing wall resistance. This effect is particularly significant in the early transient stage, when wall shear strongly influences the bulk flow.

Figures 9(a) and (b) present the volume flow rate for different t and d with $(Da = 0.1, \gamma = 0.5, \beta = 0.1, y = 0.5)$ and$(Da = 0.01, \gamma = 1.0, \beta = 0.1, y = 0.5)$. In both cases, flow rate increases with t, reflecting the establishment of the velocity field. The comparison highlights that higher $Da$and lower γ enhance flow rates due to reduced porous drag and weaker anisotropy resistance. The parameter $d$again influences interfacial coupling and the rate at which the flow approaches steady state. Figures

10(a) and (b) display the interfacial velocity profiles for varying t andβ, with $(Da = 0.1, \gamma = 1.0, d = 0.5, y = 0.4)$ and $(Da = 0.01, \gamma = 1.0, d = 0.5, y = 0.4)$, respectively. In both cases, interfacial velocity increases with time, mirroring the acceleration in both the porous and clear-fluid regions. The influence of β is once again evident: higher slip leads to larger interfacial velocities by reducing boundary-layer constraints. Moreover, higher Da enhances interfacial velocity due to reduced resistance within the porous medium.

Overall, the results consistently indicate that time evolution allows for the progressive development of velocity, reduction of skin friction, and enhancement of volume flow rate. Parameters such asDa, γ, d, and β critically shape the transient behavior by modulating porous resistance, permeability, geometric coupling, and wall-slip effects. These trends align with prior studies on unsteady flow in porous channels, where reduced resistance parameters accelerate transient response and diminish shear stresses over time.

Conclusion

This study examined the transient Couette flow in a composite channel partially filled with porous material and partially with clear fluid, using a fractional derivative framework. The Brinkman-extended Darcy model was employed for the porous region, while the Stokes equation governed the clear fluid region. The governing equations were transformed into ordinary differential equations via the Laplace transform and solved analytically using the Caputo–Fabrizio fractional derivative approach. The inverse Laplace transform was obtained using the Riemann-sum approximation. The effects of key physical parameters were analyzed and illustrated through contour plots generated in MATLAB (2016). From this research, it is found that:

i. Both the bulk velocity in the porous and clear regions and the interfacial velocity increase as time t progresses, reflecting the transient acceleration of the fluid.
ii. The wall skin frictions in both the porous and clear regions decrease with increasing time t, indicating a progressive relaxation of shear forces in the system.
iii. The volume flow rate of the unsteady Couette flow increases with time t, consistent with the velocity enhancement trend.
iv. The Caputo–Fabrizio fractional approach captures memory effects in the transient dynamics, offering a more physically realistic description compared to classical integer-order models.

v. Darcy number, slip parameter, and permeability ratio significantly influence the transient profiles, highlighting the importance of composite channel properties in controlling flow behaviour.

References

Daud, M. M., Jiann, L. Y., Mahat, R., & Shafie, S. (2022). Application of Caputo fractional derivatives to the convective flow of Casson fluids in a microchannel with thermal radiation. *Journal of Advanced Research in Fluid Mechanics and Thermal Sciences, 93*(1), 50–63. http://dx.doi.org/10.37934/arfmts.93.1.5063

Hussain, S., Qureshi, M. A., & Ahmed, S. E. (2023). Impact of wavy porous layer on the hydrodynamic forces and heat transfer of hybrid nanofluid flow in a channel with cavity under the effect of partial magnetic field. *Journal of Non-Equilibrium Thermodynamics, 48*(3), 255–269. https://doi.org/10.1515/jnet-2022-0070

Jha, B. K., & Odengle, M. Y. (2015). Unsteady Couette flow in a composite channel partially filled with porous material: A semi-analytical approach. *Transport in Porous Media, 107*, 219–234. https://doi.org/10.1007/s11242-014-0434-0

Kaurangini, M. L., & Jha, B. K. (2011). Unsteady generalized Couette flow in composite microchannels. *Applied Mathematics and Mechanics (English Edition), 32*(1), 23–32. https://doi.org/10.1007/s10483-011-1390-6

Oni, M. O., Yusuf, A. B., Yusuf, T. S., Adebayo, O. H., & Azeez, L. A. (2022). Unsteady generalized Couette flow in a horizontal channel with sudden application or removal of a porous material. *Contemporary Mathematics, 3*(2), 1365. https://doi.org/10.37256/cm.3220221365

Ranjbarzadeh, R., & Sappa, G. (2025). Numerical and experimental study of fluid flow and heat transfer in porous media: A review article. *Energies, 18*(4), 976. https://doi.org/10.3390/en18040976

Shaheen, M., Raza, A., Khursheed, H., Jameel, M., Tlili, I., Khan, S. U., Althobaiti, S. A., Gupta, M., & Khan, M. I. (2024). Applications of magnetic field and porous medium for Jeffrey (non-Newtonian) fluid using Laplace simulations. *Journal of Radiation Research and Applied Sciences, 17*(4), 101176. https://doi.org/10.1016/j.jrras.2024.101176

Singh, S. K., & Verma, V. K. (2020). Exact solution of flow in a composite porous channel. *Archives of Mechanical Engineering, 67*(1), 131685. https://doi.org/10.24425/ame.2020.131685

Verma, V. K., & Datta, S. (2012). Flow in a channel filled by heterogeneous porous medium with a linear permeability variation. *Special Topics & Reviews in Porous Media: An International Journal, 3*(3). https://doi.org/10.1615/SpecialTopicsRevPorousMedia.v3.i3.10

Verma, V. K., & Singh, S. K. (2018). Flow in a composite porous cylindrical channel of variable permeability covered with porous layer of uniform permeability. *International Journal of Pure and Applied Mathematics, 118*(2), 321–334.

Verma, V. K., & Verma, H. (2018). Exact solution of flow past a porous cylindrical shell. *Special Topics & Reviews in Porous Media: An International Journal*, *9*(1), 91–99. https://doi.org/10.1615/SpecialTopicsRevPorousMedia.v9.i1.110

Yadav, P. K., Jaiswal, S., Verma, A. K., & Chamkha, A. J. (2023). Magnetohydrodynamics of immiscible Newtonian fluids in porous regions of different variable permeability functions. *Journal of Petroleum Science and Engineering*, *220*(B), 111113. https://doi.org/10.1016/j.petrol.2022.111113